Chemistry & Biology, Vol. 9, 427–441, April, 2002, ©2002 Elsevier Science Ltd. All rights reserved. PII S1074-5521(02)00122-9

Differential Effects of FR900482 and FK317 on Apoptosis, *IL-2* Gene Expression, and Induction of Vascular Leak Syndrome

Lois Beckerbauer,[1] Jetze J. Tepe,[2] Rebecca A. Eastman,[1] Philip F. Mixter,[1] Robert M. Williams,[2,3] and Raymond Reeves[1,3]
[1]School of Molecular Biosciences
Washington State University
Pullman, Washington 99164
[2]Department of Chemistry
Colorado State University
Fort Collins, Colorado 80523

Summary

Vascular leak syndrome (VLS) is a harmful side effect that resulted in withdrawal of the antitumor drug FR900482, but not FK317, from clinical trials. Here we present chromatin immunoprecipitation data showing that FK317, like FR900482, crosslinks minor-groove binding proteins to DNA in vivo. However, these drugs differ in how they induce cell death. We demonstrate that, whereas FR900482 induces necrosis, FK317 induces a necrosis-to-apoptosis switch that is drug concentration dependent. Northern blot analyses of drug-treated cells suggest that this "switch" is mediated, at least in part, by modulation of the expression levels of Bcl-2. Additionally, FR900482, in contrast to FK317, induces the expression of known elicitors of both *Bcl-2* gene expression and VLS. These findings provide plausible explanations for why these structurally similar drugs have different biological effects, especially with respect to VLS.

Introduction

The mitosene-based antitumor drugs FR900482 and FK317 have markedly different biological side effects even though they have very similar chemical structures (Figure 1). Specifically, the FR900482 drug induces vascular leak syndrome (VLS), whereas its semisynthetic derivative FK317 does not. As a consequence, FK317 is currently in phase II clinical trials for cancer treatment in Japan as a possible new chemotherapeutic agent to potentially replace the now widely used drug mitomycin C. VLS is characterized by an increase in vascular permeability that leads to increased leakage of fluids into interstitial spaces; this leakage results in peripheral edema and, ultimately, organ failure [1–3]. Additional VLS symptoms include weight gain, hypoalbuminemia, pleural and pericardical infusion, and pulmonary and cardiovascular failure [3]. VLS has been linked to exposure to immunotoxins such as ricin A and to treatment with high concentrations of cytokines such as interleukin-2 (IL-2), as well as to various pathological conditions such as T cell lymphoma, sepsis, trauma, and burns [1, 2, 4, 5].

The semisynthetic FK317 drug is chemically modified from FR900482 by the addition of one methyl to the C5 phenolic oxygen atom and two acetyl groups (Figure 1; [6]). The acetyl groups facilitate entry of the drug into cells, but once FK317 has crossed the membrane barrier the acetyl groups are removed, producing FR157471 [7] and leaving the methyl group as the sole structural difference between it and FR900482 (see Discussion; Figure 1). Without the acetyl groups FK317 cannot be transported out of the cell by P-glycoprotein (commonly referred to as the multidrug resistance channel), thus leading to increased intracellular concentrations of the drug [8]. Both FR900482 and FK317 are prodrugs that are reductively activated inside cells. This activation occurs preferentially in the hypoxic microenvironment of solid tumors, and it is thought to proceed through a mitosene intermediate structurally similar to that formed by the reductive activation of mitomycin C [9–11]. In the reductive environment of tumor cells, FK317 is metabolized to the corresponding C12 alcohol derivative FR160516. This metabolite subsequently suffers a thiol-mediated two-electron reduction of the N-O bond to the azocine ring system, which rapidly cyclizes to the carbinolamine which, after expulsion of water, produces a highly reactive electrophilic mitosene derivative [12]. In contrast, in nontumorogenic cells, FK317 is metabolized to the C12 carboxylic acid derivative that lacks chemotherapeutic activity [6].

It is therefore important, not only from a drug design point of view but also from a biochemical perspective, to understand why two drugs of almost identical structure have such different biological effects with respect to induction of VLS and, consequently, have such different potentials as effective anticancer agents. Evidence presented here suggests that differences in the mode of action of the two drugs in inducing cell death and/or in inducing transcriptional expression of the *IL-2* gene, a known contributor to VLS, might be significant components in their differential biological effects.

Results and Discussion

Cell Growth Inhibition and Toxicity Studies

We have previously reported the effects of the FR900482 drug on the growth inhibition and toxicity of the human Jurkat acute T cell leukemia line [13]. To directly compare the effects of the FK317 drug with those of FR900482, we subcultured Jurkat cells and allowed them to grow for 24 hr before adding various concentrations (0, 0.5, 1.0, and 1.5 μM) of FK317 to the medium (Figure 2). Cell number and viability were then determined every 24 hr for the next 72 hr. As expected, a concentration-dependent effect of FK317 on cell growth (as determined by counting cell numbers) was observed with 0.5 μM of the drug being quite inhibitory to growth and with both 1.0 and 1.5 μM concentrations stopping growth all together (Figure 2). Furthermore, as discussed later, Jurkat cells treated with much higher concentrations of FK317 (10 and 100 μM) also stopped cell growth

[3]Correspondence: reevesr@wsu.edu (R.R.); rmw@chem.colostate.edu (R.M.W.)

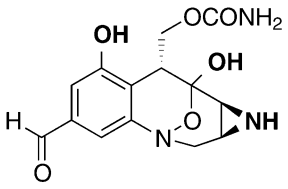

FR900482

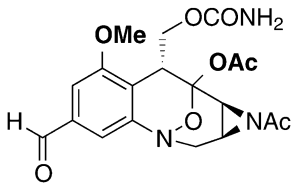

FK317

Figure 1. Chemical Structures of FK317 and FR900482

Positions at which the two structures differ are shown in bold.

within 24 hr of drug exposure. When Trypan Blue dye (2%) exclusion was used for monitoring cell viability, it was again found, as anticipated, that FK317 exhibited a concentration-dependent effect on viability (Table 1). Interestingly, as shown in Table 1, even after 24 hr treatment with 1.5 μM of the drug (i.e., at 48 hr after initiation of the experiment), an appreciable percentage of the cells in the population (>85%) was still viable even though these cells were not dividing (c.f., Figure 1). Nevertheless, after longer periods of drug treatment the viability of the cells dramatically dropped to low levels regardless of the concentration. For example, after 72 hr treatment with 1.0 μM of FK317 (i.e., 96 hr after initiation of the experiment; Table 1), only about 4% of the cells were still alive as judged by this dye exclusion assay. When these results are compared with our previous findings for the effects of various concentrations of the FR900482 drug on the same cells [13], it is obvious that FK317 is considerably more toxic to Jurkat cells. Specifically, a comparison of our previous results with those reported here indicates that 0.5 μM of FK317 causes as much inhibition of cell growth as does 1 μM of the FR900482 drug. Perhaps more importantly, after 72 hr of treatment with 1.0 μM of FK317, less than 5% of the cells are still viable (Table 1), whereas after the same length of treatment with 1.0 μM of FR900482, more than 90% of Jurkat cells are still viable [13]. Thus, in terms of cytotoxicity, FK317 appears to be a potentially more effective chemotherapeutic agent than FR900482. The difference in cellular potency may, in part, be a consequence of the two acetyl groups present on FK317, which may help this drug cross the cell membrane more efficiently than FR900482 [14], and the subsequent loss of the acetyl groups within the cell preventing the expulsion of the drug back out of the cell [8].

Protein-DNA Crosslinking Studies

A number of studies have indicated that the non-histone protein HMGA1 (formerly named HMG-I/Y; [15]), together with other transcription factors such as NF-κB and members of the Ets family (e.g., Elf-1), are involved with the in vivo transcriptional regulation of the human *IL-2* and *IL-2R*α genes as a consequence of binding to specific regions of their promoters [16–18]. Previously, we have shown that treatment of Jurkat cells with FR900482 crosslinks minor-groove binding proteins such as HMGA1, HMGB1 (formerly HMG-1) and HMGB2 (formerly HMG-2) (but not major-groove binding proteins such as NF-κB or Elf-1) to the promoter regions of the *IL-2* and *IL-2R*α genes in vivo [13]. To determine whether FK317 also makes comparable protein-DNA minor-groove crosslinks, we performed chromatin immunoprecipitation (ChIP) assays (see Experimental Procedures for details) on Jurkat cells that had been treated with 0.5 μM of FK317 for 24 hr (i.e., 48 hr after initiation of the experiment, when >90% of the cells were still viable; Table 1). In each ChIP experiment, parallel cultures of untreated Jurkat cells, or untreated cells that were fixed with 1% formaldehyde (a nonspecific crosslinker) for 30 min, served as controls. Both the experimental and control cells were then disrupted by sonication, and the resulting cellular extracts were immunopreciptated with specific antibodies against the HMGA1, NF-κB, or Elf-1 protein. After treatment to reverse any chemical crosslinks present in the immunoprecipitates, PCR primers corresponding *IL-2* and *IL-2R*α promotor regions that are reportedly bound by the HMGA1, Elf-1, or NF-kB protein in vivo were used to amplify DNA fragments present in the antibody complexes. In ChIP assays, the production of PCR products indicates that the original cellular DNA template that has

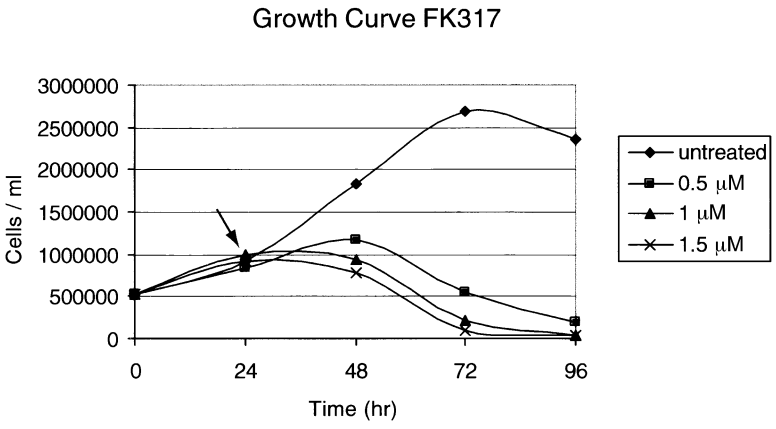

Figure 2. Growth Curves of Jurkat Cells Treated with Various Concentrations of the FK317 Drug

Jurkat cells were treated with 0, 0.5, 1.0, or 1.5 μM FK317. The number of cells in the various cultures was manually determined by hemocytometer counting. The arrow indicates the point at which the drug was added to cultures (i.e., at 24 hr after subculturing of the cells).

Table 1. Viability of Jurkat Cells Treated with Various Concentrations of the FK317 Drug According to the Protocol Shown in Figure 2

	Percent Viability			
Hr	Untreated	0.5 μM	1 μm	1.5 μm
0	100	100	100	100
24	100	100	100	100
48	98.65	93.2725	90.34	85.83
72	98.385	40.7575	18.6225	11.305
96	92.86	14.645	4.33	3.91

Cellular viability was determined by the trypan blue dye (2%) exclusion assay.

undergone amplification was crosslinked in vivo to the protein recognized by the antibody as a consequence of either direct protein-DNA or indirect protein-protein-DNA interactions. In the case of FK317- and FR900482-treated cells, indirect protein-protein-DNA crosslinks are unlikely because both drugs have been shown to preferentially react with 5′CpG-3′ sites in the minor groove of DNA [19]. The PCR products detected in the ChIP assays therefore probably result when the drugs directly crosslink minor-groove proteins to cellular DNA. Figure 3 shows the results of ChIP assays in which a specific anti-HMGA1 antibody was used for probing the promoter regions of the *IL-2Rα* (panel A) and *IL-2* (panel B) genes in Jurkat cells treated with, or without, 0.5 μM of FK317. The presence of specific amplified DNA products in the immunoprecipitates of these ChIP assays demonstrated that both the nonspecific chemical crosslinking reagent formaldehyde (lane 2; panels A and B) and the drug FK317 (lane 3; panels A and B) crosslinked the HMGA1 protein to the promoter regions of the *IL-2* and *IL-2Rα* genes in Jurkat cells. The results of several control experiments performed in parallel confirmed the specificity of these ChIP reactions. These controls produced the following results: (1) identical ChiP assays performed on cells that had not been treated with either the drug or formaldehyde showed no amplification of either *IL-2* or *IL-2Rα* gene promoter fragments (lane 4; panels A and B); and (2) PCR reactions demonstrated that specific *IL-2* (panel C) and *IL-2Rα* (data not shown) promoter fragments could be amplified from the supernatants of all of the immunoprecipitation reactions, indicating that there was ample DNA in the initial cell extracts for successful ChIP assays. Additional control ChIP experiments employing antibodies to DNA major-groove binding proteins (e.g., Elf-1 and NF-κB) also demonstrated that specific PCR products were not amplified from Jurkat cells treated (or not) with FK317 but were produced when the cells were nonspecifically crosslinked with formaldehyde (data not shown). We conclude from these data that FK317 crosslinks HMGA1 proteins to the minor groove of promoter regions of the *IL-2* and *IL-2Rα* genes in Jurkat cells in vivo. Crosslinking proteins to the DNA minor groove is, therefore, a general property of FR900482 and its derivatives and represents a novel mode of action for this class of chemotherapeutic drugs.

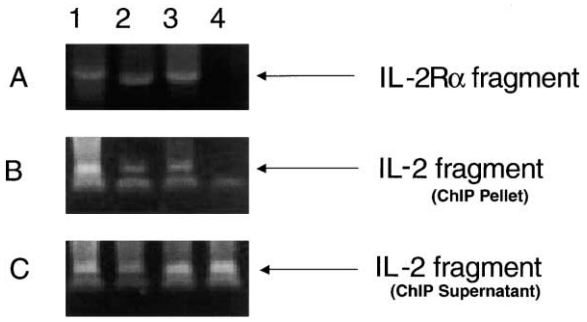

Figure 3. Agarose Gel Electrophoretic Separation of PCR-Amplified DNA Products Derived from ChIP Assays of the *IL-2* and *IL-2Rα* Gene Promoters in Jurkat Cells Treated with FK317 by the Use of an Anti-HMGA1 Specific Antibody

(A) PCR reactions performed on the pellets of the *IL-2Rα* promoter ChIP assays. Lanes are as follows: (4) control (i.e., non-drug-treated) Jurkat cells; (3) cells treated with 0.5 μM FK317 for 24 hr; (2) control (i.e., non-drug-treated) cells treated with formaldehyde, a nonspecific chemical crosslinking reagent; and (1) *IL-2Rα* promoter fragment amplified from naked Jurkat genomic DNA with the same PCR primers as those employed in the IL-2Rα ChIP reactions (specific size marker).

(B) PCR reactions performed on the pellets of the *IL-2* promoter ChIP assays. Lanes are as follows: (4) control (i.e., non-drug-treated) Jurkat cells; (3) cells treated with 0.5 μM FK317 for 24 hr; (2) control (i.e., non-drug-treated) cells crosslinked with formaldehyde; and (1) *IL-2Rα* promoter fragment amplified from naked Jurkat genomic DNA with the same PCR primers employed in the IL-2 ChIP reactions (specific-size marker).

(C) In lanes 2–4, PCR products were obtained from the supernatants of the same ChIP reactions shown in panel B. Using *IL-2* primers confirmed that all of the cellular extracts contained amplifiable DNA. In lane 1, a positive *IL-2* size control fragment amplified from naked DNA is shown. The lower of the two bands present in both panels B and C are primer-dimer amplification artifacts.

Apoptosis versus Necrosis: Differential Effects of FK317 and FR900482

The two most thoroughly characterized modes of cell death are apoptosis and necrosis. Both pathways can be triggered by a wide variety of factors and lead to the same end—total cell degeneration. There are marked differences, however, in both the morphological characteristics and the cellular pathways involved in the two modes of death. For example, apoptosis usually occurs in single cells and rarely do all the cells in one area of an organ or tissue undergo death at the same time, whereas necrotic cell death involves large groups of cells and sometimes even entire organs or tissues. Furthermore, as shown in diagram A of Figure 4, one of the first detectable changes in a cell undergoing apoptosis, as opposed to necrosis, is noticeable cytoplasmic shrinkage (reviewed in [20]). This is soon followed by changes in intracellular Ca^{2+} and ATP levels, loss of mitochondrial membrane potential, and activation of proteolytic caspases. Concomitant with these changes, fragmentation of the nuclear DNA occurs (Figure 4A) and is followed by reorientation of phosphatidylserine from the inner to the outer surface of the cytoplasmic membrane (Figure 4B). The cellular cytoplasm and degraded organelles finally bleb off into apoptotic bodies, and the cell degenerates (Figures 4C and 4D). Macrophages and other types of phagocytic cells target the

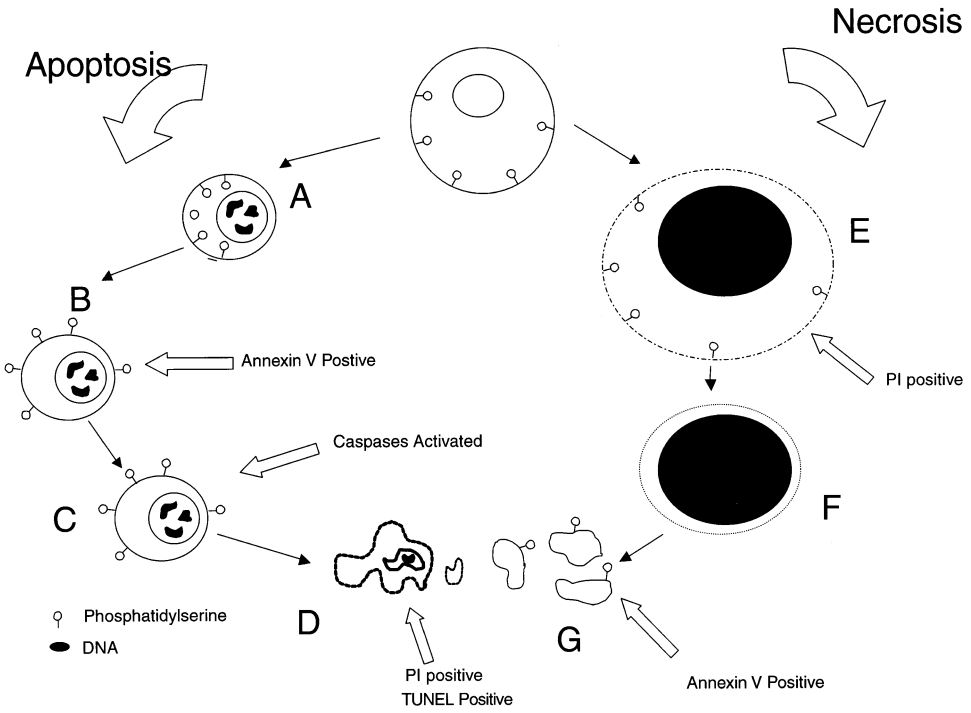

Figure 4. A Schematic Diagram of Necrosis and Apoptosis Indicates when, during the Death Process, Cells Stain Positive for Annexin-V-FITC and PI

Cells labeled A and B are in the early stage of apoptosis, whereas those labeled C and D are in the late stage. Cells labeled E are in the early stage of necrosis, whereas those labeled F and G are in the late stage. Cells undergoing apoptosis fragment their DNA/chromatin and shrink in size early during the death process (A). Also during the early stages of apoptosis, phosphatidyl serine, which is normally situated on the inner surface of the cytoplasmic membrane, flips to the outside (B), and the cells become Annexin-V positive when stained with Annexin-V-FITC. Subsequently, their membranes become permeable, the cells bleb off apoptotic bodies, and their DNA fluoresces red when stained with propidium iodide (i.e., they become PI positive). Apoptotic cells at this late stage fluoresce both green and red and are TUNEL positive when assayed for DNA fragmentation. In contrast, the early stages of necrotic cell death are characterized by the swelling of both the cytoplasm and the nucleus of cells, as well as by marked chromatin condensation (E). As a consequence of the loss of cytoplasmic membrane integrity, the DNA of early necrotic cells fluoresces red when the cells are stained with PI (E). Shortly afterwards, the cells begin to lose cytoplasm (F) and finally become Annexin-V positive at the later stages of the necrosis process, producing cell fragments that fluoresce both red and green (G).

apoptotic cell remnants after detecting changes in these cells' outer cytoplasmic membrane. The phagocytes engulf and degrade the apoptotic debris of individual cells and thus prevent inflammation [21–24].

In contrast to apoptosis, the early morphological events that accompany cellular death by necrosis are cytoplasmic and nuclear enlargement and condensation of chromatin (Figure 4E). There is also a rapid loss of the integrity of the cytoplasmic membrane (Figures 4E and 4F) and an eventual loss of cytoplasm into the extracellular space (Figure 4F). This loss of cytoplasm is the result of cations moving from the interior to the exterior of the cell. As a consequence of this cation flux and other pathological changes, extracellular fluids enter into the cell and cause it to swell and eventually rupture into fragments (Figure 4G) that are engulfed and degraded by phagocytes. Due to the loss of cytoplasm into the extracellular space and to the fact that large numbers of cells usually undergo simultaneous degeneration in the same localized area of an organ or tissue, inflammation usually accompanies necrotic cell death [21–24].

We have previously demonstrated that FR900482 induces necrotic cell death in Jurkat cells regardless of the drug concentration employed [13]. However, for a chemotherapeutic agent, an apoptotic mode of cell death is preferred because necrosis sometimes leads to severe inflammation and serious side effects such as VLS. We were therefore interested in determining whether the FK317 derivative of the FR900482 drug also caused necrosis or if the structural difference(s) altered its biological action and mode of cell death.

Flow cytometry using fluorescein-isothiocyanate (FITC)-labeled Annexin-V and propidium iodide (PI) allows one to experimentally distinguish among early apoptotic, early necrotic, and late apoptotic/late necrotic events (c.f., Figure 4). Cells that are undergoing apoptosis "flip" phosptidylserine from the inside to the outside of the cytoplasmic membrane leaflet early in the death pathway (Figure 4B), which allows Annexin-V, a natural substrate of phosphatidyl serine, to bind to the outer membrane of the cells. Thus, in time-course staining experiments, cells undergoing apoptotic death will first stain with Annexin-FITC and fluoresce green when analyzed by a flow cytometer. Only at later stages of the death process, when the cytoplasmic membrane becomes permeable, will apoptotic cells fluoresce red

as a result of PI binding to DNA (Figure 4D). A reverse sequence of fluorescence staining events is observed for cells undergoing necrosis. Early during necrosis, cells first stain red with PI as a consequence of early membrane permeability changes (Figure 4E) and only later stain green with Annexin-V-FITC as a result of the exposure of phosphatidyl serine on the outer surface of the cytoplasmic membrane (Figure 4G; [25, 26]).

As schematically shown in Figure 5A, the readout of fluorescence intensities from flow cytometric analyses employing Annexin-V-FITC/PI double staining of cells in time-course experiments can be used to determine whether drug treatments induce apoptotic or necrotic cell death. In this diagram, increasing intensity of green Annexin-V-FITC fluorescence is plotted on the horizontal (*x*) axis, and increasing intensity of red PI fluorescence is plotted on the vertical (*y*) axis. Thus, in flow cytometric experiments, viable (i.e., untreated, control) cells will exhibit little red or green fluorescence and will cluster in the lower left-hand quadrant of the flow cytometry screen, whereas drug-treated cells undergoing early necrosis will exhibit increased relative amounts of red:green fluorescence and will cluster in the upper left-hand quadrant of the screen (Figure 5A). Correspondingly, early apoptotic cells will cluster in the lower right-hand portion of the flow cytometry screen because of increased green:red fluorescence, and both late necrotic and late apoptotic cells will cluster in the upper right-hand quadrant of the screen (Figure 5A). The numbers of cells (each dot represents one cell) in the different flow-cytometric quadrants therefore represent the proportion of cells undergoing different modes of cell death in a population.

In time-course experiments to distinguish between necrotic and apoptotic cell death, the FR900482 and FK317 drugs were added to Jurkat cells at 1, 10, and 100 μM concentrations and incubated for 24, 48, or 72 hr before flow-cytometric analysis. Quadrant settings were determined for each experiment based on controls that were simultaneously run in parallel; therefore the actual quadrant lines varied somewhat from experiment to experiment (Figure 5). Regardless of the settings, however, the results of these carefully controlled time-course experiments reproducibly demonstrated that Jurkat cells treated with FR900482 first increased their red PI staining intensity and only later became positive for green Annexin-V-FITC staining (data not shown), thus confirming our earlier observations that this drug induces necrotic cell death in a concentration-independent manner [13]. In contrast, as illustrated by the representative flow-cytometric analyses shown in panels B–H of Figure 5, the mode of death induced by the treatment of Jurkat cells with FK317 depends on the drug concentration employed. For example, in comparison to untreated controls (panel B), after 24 hr of treatment with 1 μM of FK317, a significant fraction of the Jurkat cells had increased their relative PI red fluorescence intensity as indicated by their shift to the upper-left quadrant (panel E), whereas at a later time (72 hr) they had increased both their red and green intensities and shifted to the upper-right quadrant (panel F). This characteristic time course of changes in relative red:green fluorescence intensities indicates that at low concentrations the FK317 drug induces cellular necrosis. In marked contrast, cells treated with 10 μM FK317 for 24 hr (panel G) and 72 hr (panel H) first shift to the lower-right quadrant and then to the upper-right quadrant, indicating that at a 10-fold higher concentration the drug induces changes characteristic of apoptotic cell death. Likewise, the FK317 drug also induces apoptotic cell death at even higher drug concentrations (e.g., 100 μM; Figures 5I–5K; unpublished data).

In order to better compare the responses of Jurkat cells exposed to different concentrations of FR900482 and FK317 drugs, we performed flow-cytometric analyses in triplicate and graphed the percentage of cells found in each quadrant as a function of time of drug treatment (Figures 5I–5K). These experiments demonstrated that the percent of cells staining as early necrotic (i.e., upper-left quadrant) was high for cells treated with either 1 μM FK317 or 10 μM FR900482 (panel I), as well as all other concentrations of the FR drug used (data not shown). In contrast, the percent of apoptotic cells after treatment with either 1 μM FK317 or 10 μM FR900482 was low (panel J). From these graphs it is also evident that for cells treated with 1 μM FK317 the percent of early necrotic cells decreased with time (panel I). This decrease in the percent of necrotic cells can be accounted for by a corresponding increase in the percent of late necrotic/late apoptotic cells at later time points (panel K). In contrast, cells treated with 10 μM FR900482 did not exhibit changes in their percent necrotic death over time (panels I and K). Most significantly, however, it should be noted that the percent of early necrotic cells was very low for both 10 and 100 μM FK317 (panel J), whereas the percent of early apoptotic cells at these drug concentrations was high (panel J). These same drug-treated populations also exhibited an increase in the percent of late necrotic/late apoptotic cells with time (panel K) while showing a decrease in their percent of early apoptotic cells (panel J). Therefore, the cumulative data from these flow cytometric analyses indicate that cells treated with high concentrations (10 and 100 μM) of FK317 become more apoptotic with time, whereas those treated with the lowest concentration (1 μM) of this drug became more necrotic. Thus, a necrosis-to-apoptosis switch occurs in Jurkat cells treated with different concentrations of the FK317, but not the FR900482, drug.

As an independent method for verifying the flow cytometric data, drug-treated cells were double-stained with hematoxylin and Giemsa, and their morphology (c.f., Figure 4) was examined for features that are characteristic of either necrosis or apoptosis (Figure 6). In comparison to untreated Jurkat cells (Figure 6J), cells treated with 1 μM FK317 (Figures 6A–6C) or 1 μM FR900482 (see Figure 5 of reference [13]) became enlarged, lost cytoplasmic integrity, and underwent nuclear condensation. These morphological changes are indicative of a necrotic mode of cell death. In contrast, Jurkat cells treated with either 10 or 100 μM FK317 (Figures 6D–6I) exhibited nuclear fragmentation (panel D) and the formation of apoptotic bodies (panels E–I), morphological features characteristic of death by apoptosis. The results from two independent experimental methods, flow-cytometric analysis and cytological examination, are

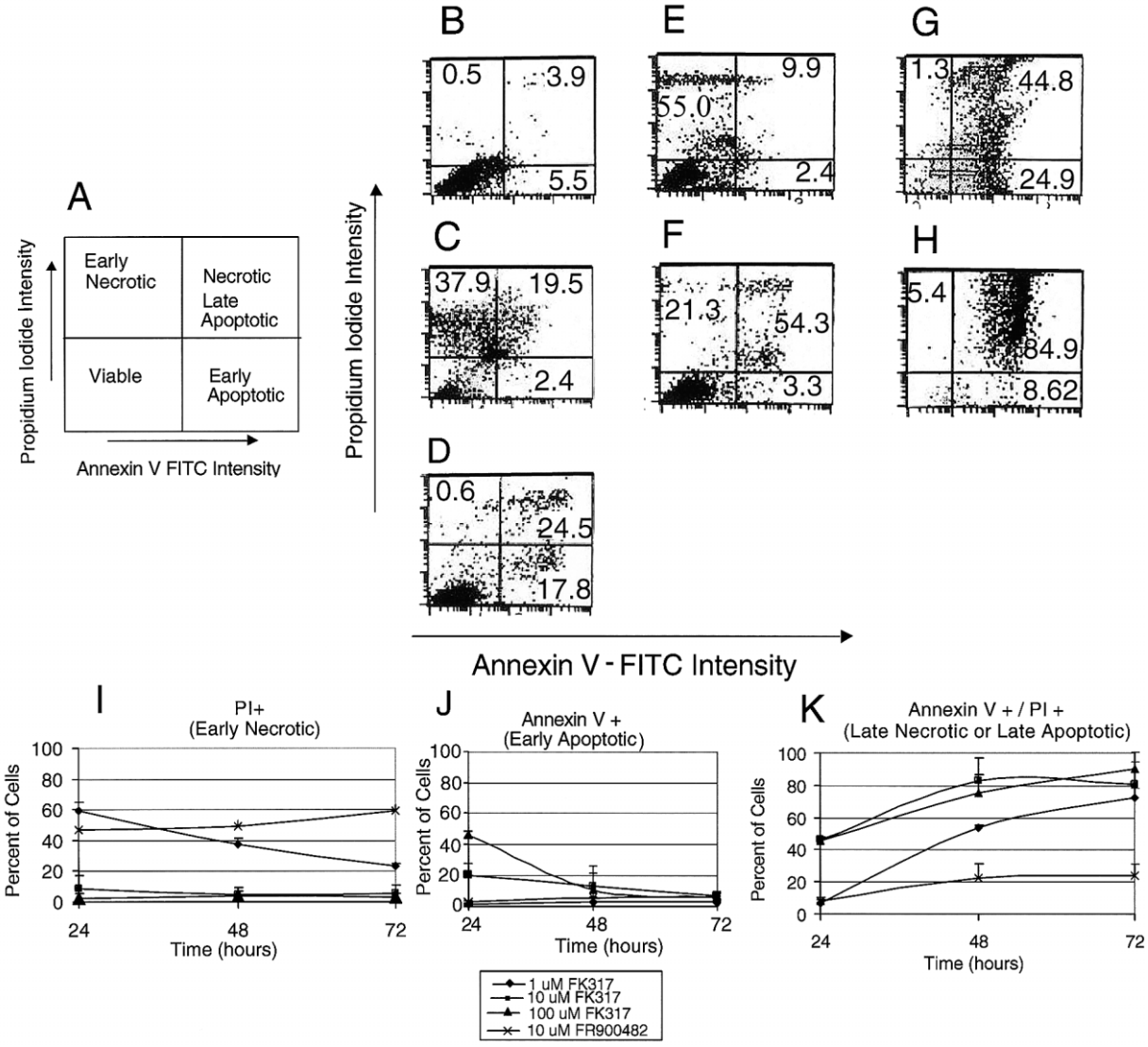

Figure 5. Flow Cytometric Analysis of Jurkat Cells Treated with Various Concentrations of FK317 and Stained with Annexin-V-FITC and PI

Annexin-V-FITC staining appears as green fluorescence, and PI staining appears as red fluorescence. Panel (A) shows a schematic of a flow cytometry grid indicating into which quadrant cells that are viable, early necrotic, early apoptotic, or late apoptotic/late necrotic would fall (see text for discussion). Arrows depict increasing red (*y* axis) or green (*x* axis) fluorescence. Panels (B–H) show representative flow-cytometric analyses (the data in each panel are derived from an independent, appropriately controlled experiment) of cells that were treated with different concentrations of FK317 for different periods of time. Each panel shows a representative analysis based on at least three separate experiments. The numbers in each quadrant indicate the percentage of cells in the population in that quadrant. Jurkat cells were (B) left untreated (i.e., no drug control); (C) treated with 10% EtOH (an inducer of necrosis) for 10 min; (D) treated with 1 μM mitomycin C (an inducer of apoptosis) for 72 hr; (E) treated with 1 μM FK317 for 24 hr or (F) for 72 hr; or (G) treated with 10 μM FK317 for 24 hr or (H) 72 hr. Panels (J–K) are Excel-derived graphs of these flow cytometry results and show the percentage of cells present in each quadrant as a function of both drug concentration and time of treatment. Panel I shows the percent of early necrotic cells, panel J shows the percent of early apoptotic cells, and panel K shows the percent of late necrotic/late apoptotic cells. It should be noted that, regardless of the time of treatment, at a concentration of 1 μM of FK317 and 10 μM of FR900482 the percent of early necrotic cells was relatively high, whereas the percent of early apoptotic cells was very low. In contrast, for cells treated with either 10 μM or 100 μM FK317, the percent of necrotic cells was very low, whereas the percent of apoptotic cells was high. As discussed in the text, these results indicate that at low concentrations the FK317 drug preferentially induces necrotic cell death, whereas at high concentrations it induces apoptosis.

therefore in agreement and indicate that, whereas FR900482 induces necrosis in Jurkat cells at all concentrations tested, the FK317 drug causes a concentration-dependent switch from necrosis to apoptosis.

To further investigate the validity of these unanticipated results, we employed a third widely used method for determining the mode of cell death, the TUNEL assay. The TUNEL assay involves the in situ addition of fluorescently labeled deoxyuridine triphosphate (dUTP) to the free ends of damaged DNA in the nuclei of permeabilized cells by the use of the enzyme terminal deoxynucleotidyl transferase (see Experimental Procedures). Therefore,

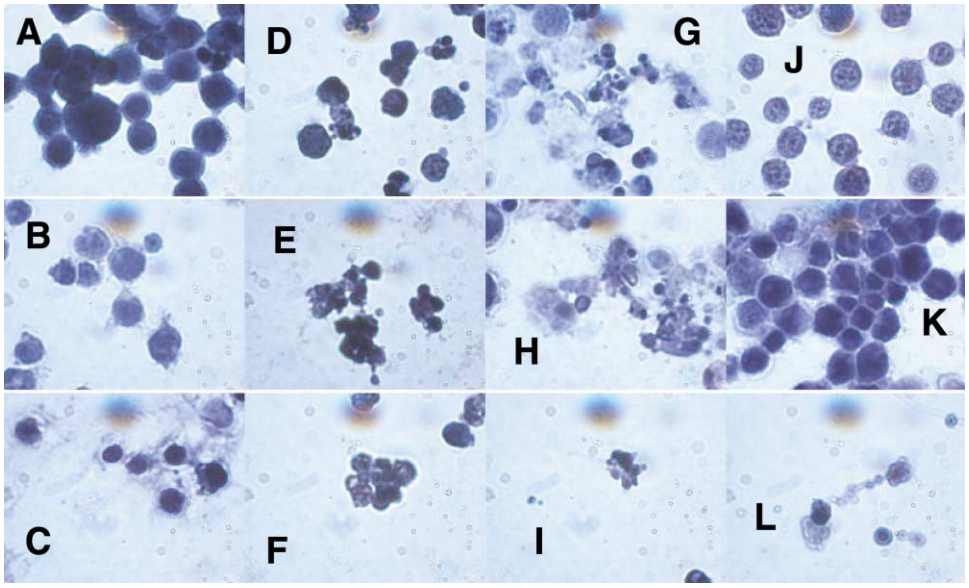

Figure 6. Cytological Confirmation of the Dose-Dependent Effects of FK317 on the Induction of Cellular Necrosis and Apoptosis

Gross morphology (100× magnification) of Jurkat cells treated with 1 μM (A–C), 10 μM (D–F), or 100 μM (G–I) of FK317 for 24 (A, D, and G), 48 (B, E, and H), or 72 (C, F, and I) hr and double-stained with hemotoxylin (purple; nucleus) and Giemsa (blue; cytoplasm). Panel J shows untreated cells. Cells treated with 1 μM FK317 (A–C) first become swollen, undergo nuclear chromatin condensation, and then loose cytoplasmic integrity, indicating that they are undergoing necrosis. Those cells treated with 10 (D–F) and 100 (G–I) μM FK317 exhibit chromatin fragmentation (D) and have formed apoptotic bodies (E–I), indicating that they are undergoing apoptosis. The gross morphology of Bcl-2-overexpressing Jurkat cells that have been treated with 100 μM FK317 for either 24 (K) or 72 (L) hr demonstrates that such cells first become swollen and then lose their cytoplasmic integrity in a manner similar to that of Jurkat cells that are undergoing necrotic cell death after treatment with 1 μM FK317 (A–C).

the nuclei of cells undergoing DNA fragmentation as a consequence of apoptosis are fluorescently labeled in TUNEL assays, whereas those undergoing death by necrosis are not. Importantly, in comparison to the Annexin-V-FITC assay, which detects the early stages of apoptosis, TUNEL assays detect only the late DNA fragmentation events associated with apoptosis (c.f., Figure 4); thus, the two methods represent complementary ways of assessing apoptotic cell death. TUNEL assays were performed on Jurkat cells treated with 1 μM, 10 μM, and 100 μM FK317 for 24 hr and, as expected from our earlier findings, the nuclei of cells treated with 1 μM were not labeled by the enzymatic incorporation of fluorescent dUTP, whereas those treated with 10 and 100 μM were (data not shown). These results indicate that, in agreement with both the Annexin-V-FITC data and the cellular morphology data, Jurkat cells treated with 10 μM and 100 μM FK317 undergo an apoptotic cell death, whereas those treated with 1 μM FK317 do not.

As a final approach to assessing the mode of death in drug-treated cells, we performed experiments to determine whether the caspase proteolysis cascade is activated in cells treated with either FK317 or FR900482. Caspase activation is an apoptotic-cell characteristic that occurs sometime between when dying cells become Annexin-V-FITC positive and when they become TUNEL positive (c.f., Figure 4). Jurkat cells were treated for 24 hr with 1 or 10 μM of either FK317 or FR900482, collected by centrifugation, and then resuspended and incubated in a buffer containing the dye Phi Phi Lux. Phi Phi Lux, a peptide substrate for the downstream (effector) caspases 3 and 7, fluoresces red when cleaved by proteolysis. This increased red fluorescence, which is indicative of the activation of cellular apoptosis, is easily detected and measured by flow cytometry (see Experimental Procedures). The flow cytometry results shown in Figure 7 demonstrate that neither cells treated with 1 or 10 μM of FR900482 (panels D and E) nor those treated with 1 μM of FK317 (panel B) exhibited red fluorescence above the background observed in control Jurkat cells that have not been exposed to drugs (panel A). In contrast, Jurkat cells treated with 10 μM FK317 (panel C) exhibited a marked increase in red fluorescence, as indicated by the shift of a significant number of cells into the area marked M1 in the flow diagram. These data clearly indicate that apoptosis-inducing caspases have been activated in cells treated for 24 hr with 10 μM FK317 but not (as expected for necrotic cells) in cells treated with either 10 μM FR900482 or 1 μM FK317 for the same time period.

In the context of chemotherapeutic agents, necrosis is generally thought to be the consequence of acute cellular toxicity, and an apoptosis-to-necrosis switch is often observed when one goes from lower to higher concentrations of drugs. Therefore, the switch in the opposite direction, from necrosis-to-apoptosis, that we observed with the FK317 drug was unexpected and initially surprising, but not unprecedented. Recently, Palomba et al. [27] found a similar necrosis-to-apoptosis switch when U937 cells were treated with H_2O_2 and the poly (ADP-ribose) polymerase (PARP) inhibitor 3-aminobenzamide (3AB). These authors found that when U937

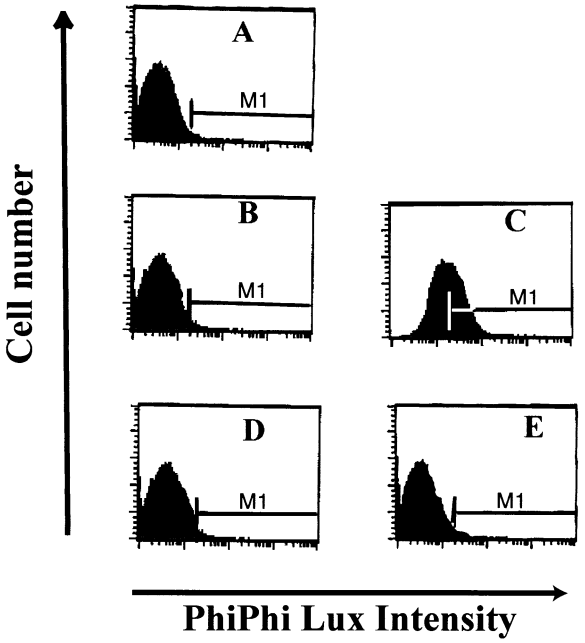

Figure 7. Induction of Apoptosis Effector Caspases 3 and 7 in Cells Treated with FK317

Jurkat cells were either left untreated (A) or treated for 24 hr with 1 μM (B) or 10 μM (C) FK317 or with 1 μM (D) or 10 μM (E) FR90082. The cells were then incubated with the peptide Phi Phi Lux, a substrate for the downstream effector caspases 3 and 7 that fluoresces upon proteolytic cleavage, and the treated cells were analyzed by flow cytometry. It should be noted that, as demonstrated by the shift of cells into the area marked M1, a significant number of cells treated with 10 μM FK317 exhibit increased red fluorescence (C) indicative of the activation of apoptosis-inducing caspases within 24 hr of drug treatment. The placement of M1 was determined by the negative control (A).

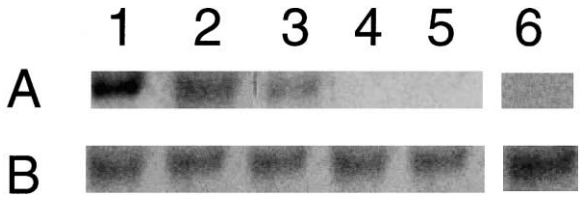

Figure 8. Northern Blot Analysis of mRNA Isolated from FK317- and FR900482-Treated Jurkat Cells with *Bcl-2* and *Gapdh* cDNAs as Hybridization Probes

(A) *Bcl-2* probe; (B) *Gapdh* probe. RNA was isolated from Jurkat cells that were treated with 1 μM FR900482 (lane 1), 100 μM FR900482 (lane 2), 1 μM FK317 (lane 3), 10 μM FK317 (lane 4), or 100 μM FK317 (lane 5) or left untreated (lane 6). The cells were then separated by electrophoresis on a formaldehyde agarose gel, transferred to a nylon membrane, and probed by hybridization. It should be noted that *Bcl-2* message (A) is high in cells treated with 1 and 100 μM FR900482 (lanes 1 and 2), decreased in those cells treated with 1 μM FK317 (lane 3), and is undetectable in cells treated with 10 and 100 μM FK317 (lanes 4 and 5) as well as in untreated control cells (lane 6). The levels of *Gapdh* message remained essentially constant in both control cells and cells treated with various concentrations of drugs (B).

cells were treated with a constant amount of 3AB and increasing concentrations H_2O_2, cellular necrosis occurred at low hydrogen peroxide concentrations, whereas apoptosis occurred at higher concentrations. Treatment of cells with 3AB alone did not induce apoptosis. From these data, Palomba and colleagues concluded that an active necrotic cell death pathway exists in U937 cells and that this pathway is modulated by the inhibitor 3AB. They also hypothesized that an active necrotic death pathway exists in other cell types, as well.

The argument for a necrotic cell death pathway is made stronger by the facts that cellular mechanisms that signal either early necrosis or apoptosis overlap and that it is only due to slight fluctuations in one direction or the other that leads to either apoptosis or necrosis [28, 29]. One such mechanism is the mitochondria permeability transition. It has been argued that similar changes relating to the mitochondria permeability transition occur in both early necrosis and early apoptosis [22]. This transition involves the formation of regulated megachannels within a dynamic ensemble of proteins that cross both the inner and outer membranes of the mitochondria. The opening of this channel during apoptosis causes the release of solutes that are larger than 1500 kDa and results in the loss of mitochondrial RNA, proteins, and function [22]. Effectors of this permeability include ions, nucleotides, and lipids, all of whose levels change markedly during apoptosis or necrosis [22, 30]. When this transition causes bioenergetic and redox changes, necrosis is induced, but when it causes the release of cytochrome C, Apoptosis-Inducing Factor (AIF), and other death-inducing factors, apoptosis results [22, 24]. It therefore seems reasonable, if one assumes that a necrotic cell death pathway does exist in all cells, that a "switch" could easily occur during the death initiation process to direct a cell toward either necrosis or apoptosis, depending on which proteins and other stimuli are associated with the mitochondria permeability transition.

Bcl-2 Proteins and the Necrosis-to-Apoptosis Switch

A possible explanation for the necrosis-to-apoptosis switch we observed is that cellular levels of the anti-apoptotic protein Bcl-2 change depending on drug concentration. The Bcl-2 proteins are major players in determining which mode of cell death the mitochondrial permeability transition causes. Additionally, in Jurkat cells it has been demonstrated that mitochondria are required for the activation of downstream caspases during apoptosis activation and also that Bcl-2 can inhibit apoptosis [31]. Members of the Bcl-2 protein family (including Bcl-2, Bax, Bcl-x, Bak, Bad, and MCl-2) have the ability to homodimerize, to heterodimerize with other members of the Bcl-2 family, and also to bind to other nonhomologous proteins. The biological function of Bcl-2 complexes is dependent on their composition and influences—for example, the formation of ion channels and pores [32]. Overexpression of Bcl-2 inhibits the efflux of cytochrome C from mitochondria and thereby prevents apoptosis [24]. This, in turn, preserves caspase 3 in its inactive state and thereby prevents the cleavage of death pathway substrates and the downstream molecular cascade that leads to apoptosis [33]. This inhibi-

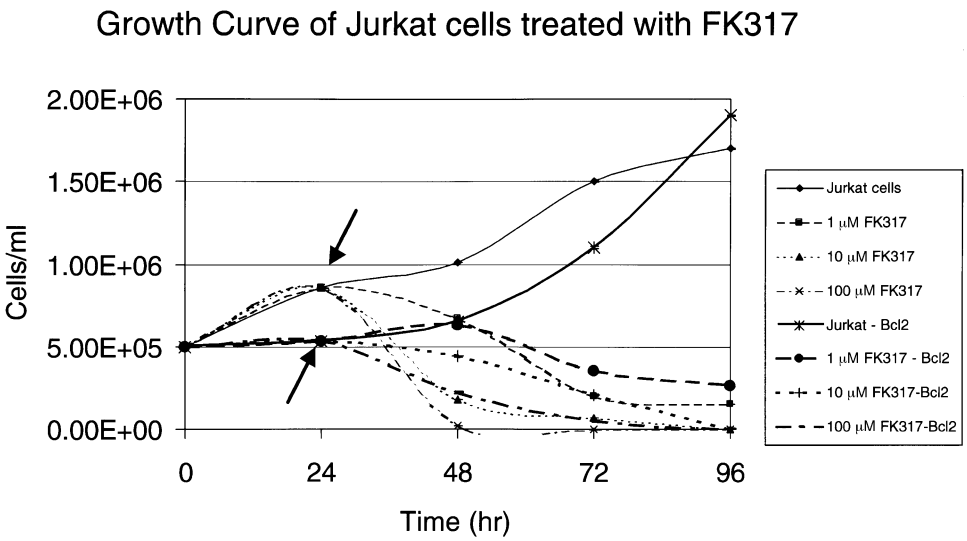

Figure 9. Growth Characteristics of Bcl-2-Overexpressing Jurkat Cells Treated with Various Concentrations of the FK317 Drug

The number of cells in the various cultures was manually determined by hemacytometer counting. The arrow indicates the point at which drug (0, 1, 10, or 100 μM) was added to cultures (i.e., at 24 hr after subculturing of the cells).

tion of apoptosis has been shown to be due to the formation of Bcl-2 homodimers in cells. In contrast, when Bcl-2 forms hetereodimers with other proteins, such as Bax, it promotes apoptosis [34]. Therefore, the ratio of Bcl-2 homodimers to hetereodimers plays an important role in the determining whether apoptosis or necrosis occurs. High cellular levels of Bcl-2 lead to the formation of more homodimers, which in turn results in the inhibition of apoptosis [32, 35, 36, 33]. In contrast, at low cellular levels of Bcl-2, this ratio is likely to decrease and thereby promote apoptosis.

To investigate whether Bcl-2 proteins participate in the differential effects of the FR900482 and FK317 drugs on Jurkat cells, we isolated mRNA from drug-treated cells and probed them by Northern blot analysis for *Bcl-2* message. The cDNA probe for *Bcl-2* used in these experiments was specific for both Bcl-2α and its truncated isoform, Bcl-2β, but did not detect any other members of the Bcl-2 family. However, owing to its size, the band observed on Northern blots corresponds to the *Bcl-2*α isoform and not to the β isoform (data not shown). Thus, when we refer to Bcl-2 we mean the α isoform. As shown in Figure 8, the levels of *Bcl-2* mRNA differed markedly between cells treated for 24 hr with FR900482 and those treated with FK317. FR900482-treated cells had the highest levels of *Bcl-2* message (Figure 8A, lanes 1 and 2), whereas the *Bcl-2* message levels in cells treated with 1 μM FK317 were considerably reduced (Figure 8A, lane 3) and were undetectable in cells treated with either 10 or 100 μM FK317 (Figure 8A, lane 4–5). In comparison to untreated Jurkat cells (Figure 8A, lane 6), cells treated with all concentrations of FR900482 or with 1 μM FK317 had higher levels of *Bcl-2* expression. The levels of mRNA of a control housekeeping gene, *Gapdh*, remained constant in all of the cells (Figure 8B), demonstrating that equal amounts of mRNA were analyzed in these experiments. It should be stressed that several recent papers have shown a direct correlation between the cellular levels of Bcl-2 protein and the levels of *Bcl-2* mRNA [37, 38]. Therefore, it is likely that the mRNA increase we observe here directly leads to increasing amounts of Bcl-2 protein in the drug-treated cells. In addition, a correlation between increased levels of *Bcl-2* mRNA and decreased apoptosis has been demonstrated [39]. In light of these data, it can therefore be hypothesized that in cells treated with various concentrations of FR900482 or with low levels of FK317, the Bcl-2 homodimer/hetereodimer ratio is high and that it is this elevated ratio that is preventing cells from undergoing apoptosis. Nevertheless, it is also likely that these same drug-treated cells have accumulated enough damage as a consequence of drug-induced DNA-protein and/or DNA-DNA crosslinks that necrotic death is triggered. A finding consistent with this hypothesis is the fact that, as shown in Figure 8A, cells treated with higher concentrations of FK317 (10 μM, lane 3; 100 μM, lane 4) have undetectable levels of *Bcl-2* mRNA. This suggests that in cells treated with these higher FK317 concentrations, the endogenous Bcl-2 homodimer/hetereodimer ratio is considerably lower than in cells treated with FR900482 (or low levels of FK317), thereby causing signals such as cytochrome C and AIF to be released from mitochondria that induce apoptotic cell death.

To further investigate the possible involvement of Bcl-2 in the necrotic/apoptotic switch induced by FK317, we investigated drug-induced cell death in transgenic Jurkat cells that were overexpressing the Bcl-2 protein (Jurkat-Bcl2 cells) [40]. If, as speculated, the cellular levels of Bcl-2 protein are indeed mechanistically associated with the necrosis-to-apoptosis switch, a difference in the mode of cell death and/or detectable changes in the degree of cellular toxicity would be predicted for Jurkat-Bcl2 cells, compared to the parental Jurkat cells, that are treated with increasing concentrations of FK317. To determine whether such altered cellu-

lar responses are observable, we used growth curves to compare the proliferation rates of both the Jurkat and Jurkat-Bcl2 cells in the presence of 1, 10, and 100 μM of either FK317 or FR900482 (Figure 9 and data not shown). As anticipated, no differences were observed between the growth rates of the Jurkat and Jurkat-Bcl2 cells that were treated with FR900482 because this drug induced necrotic death at all of the concentrations used (data not shown). In contrast, Jurkat-Bcl2 cells that were treated with higher concentrations of FK317 (10 and 100 μM) exhibited noticeably greater proliferative capacity than the parental Jurkat cells at each of the drug concentrations (Figure 9). Trypan blue dye exclusion viability assays also indicated that the drug-treated Jurkat-Bcl2 cells died at a somewhat slower rate than the normal Jurkat cells at high drug concentrations (data not shown), suggesting that they were somehow "protected" from FK317-induced cell death. It is reasonable to speculate that the increased levels of Bcl-2 protein present in the Jurkat-Bcl2 cells provided this "protection" by inhibiting the apoptotic death pathway and thus forcing the cells to die by necrosis. To confirm that, in this case, such a switch between drug-induced apoptosis and necrosis did occur in these cells, we examined the morphology of Jurkat-Bcl2 cells that had been treated with 1, 10, or 100 μM FK317 and stained with hemetoxylin and Giemsa (Figures 6K and 6L and data not shown). The overall morphology of these drug-treated cells had clearly changed from that of apoptotic cells (Figures 6D–6I) to that of necrotic cells, as demonstrated by the fact that by 24 hr of drug treatment they had become noticeably swollen (Figure 6K) and by 72 hr had lost their cytoplasmic integrity (Figure 6L). Together, these data are consistent with the proposal that Bcl-2 plays an important role in determining the mode of cell death and in inducing the necrotic/apoptotic switch caused by FK317. Furthermore, the results provide a cautionary note that the concentrations of FK317 drug employed for cancer therapeutic purposes should be optimized to ensure the induction of apoptotic, rather than necrotic, death of tumor cells.

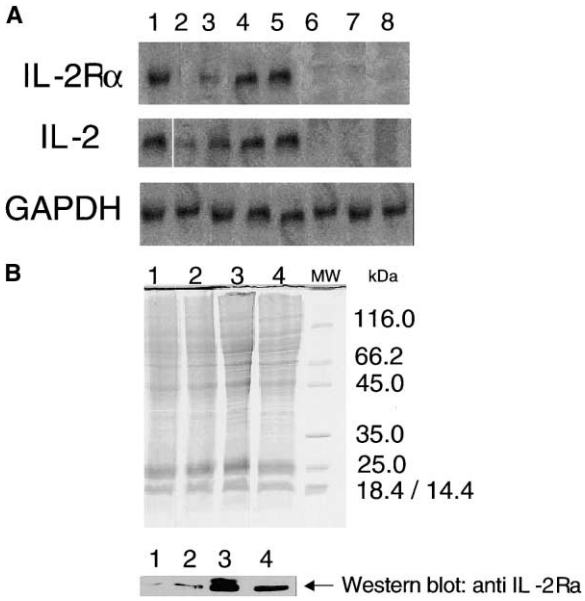

Figure 10. Northern and Western Blot Analyses of FK317- and FR900482-Treated Jurkat Cells with, respectively, either *IL-2Rα*, *IL-2*, or *Gapdh* Hybridization Probes or Anti-IL-2Rα Antibody

(A) Northern blot. RNA was isolated from Jurkat cells treated with 1 μM FR900482 (lanes 3–5) or 1 μM FK317 (lanes 6–8) for 6 hr (lanes 3 and 6), 12 hr (lanes 4 and 7), or 24 hr (lanes 5 and 8). For negative and positive controls of *IL-2* and *IL-2Rα* mRNA induction, Jurkat cells were, respectively, left untreated (lane 2) or treated with a combination of PMA/Con A for 24 hr (lane 1). RNA was isolated and analyzed as in Figure 8 except that probes for the *Il-2Rα* (exon 1), *Il-2* (3′ UTR), and *Gapdh* cDNA were used.

(B) Western blot analysis of total proteins isolated from either untreated Jurkat cells (lane 1) or cells treated with 1 μM FK317 (lane 2), 1 μM FR900482 (lane 3), or a combination of PMA/Con A (lane 4). The gel in the top of panel B was stained with Coomassie blue and demonstrates equal protein loading in all of the lanes. The lane labeled MW on the right contains standard molecular-weight protein markers (sizes in kDa are indicated on the side) for comparison. The lower part of panel B shows a Western blot of a portion of a gel, identical to that shown above, reacted with a specific anti-IL-2Rα antibody. Note that FK317-treated cells (lane 2) contain approximately the same amount of IL-2Rα protein as untreated control cells (lane 1), whereas FR900482-treated cells (lane 3) contain greatly increased levels of protein—more, even, than Jurkat cells stimulated with the potent IL-2Rα protein-inducing combination Con A/PMA (lane 4).

Differential Drug-Induction of *IL-2* and *IL-2Rα* mRNAs

Early in our investigations we suspected that the previously discussed differential induction of VLS by FR900482, but not by FK317, was likely to be mediated by mechanisms or factors other than the differences in the modes of cell death caused by the two drugs. One possibility, for example, would be for the two drugs to differentially affect the expression of cytokines, such as IL-2, that others have directly linked to the induction of VLS [3]. Supportive of this idea is the fact that when IL-2 adjuvant therapy was first used for cancer treatment, VLS was a major detrimental side effect [3, 41]. The induction of VLS by IL-2 treatment has been suggested to be a consequence of IL-2 activation of the adherence of neutrophils to endothelial cells and the release of reactive oxygen intermediates and proteases from the bound neurtrophils that initiate lysis of the endothelial cells [3, 42]. Based on this proposed scenario, a reasonable hypothesis to explain why FR900482 induces VLS, and FK317 doesn't, is that only FR900482 induces the expression of IL-2.

To test this hypothesis, we performed Northern blot analyses to determine the *IL-2* and *IL-2Rα* mRNA levels present in cells treated with 1 μM of either the FR900482 or the FK317 drug for 6, 12, and 24 hr to compare the levels of these messages found in untreated control cells. As a positive control for these experiments, mRNA was also isolated from cells that were treated with phorbol 12-myristate 13-acetate (PMA) plus concanavalin A (Con A), a combination of stimulatory agents known to induce transcription of the *IL-2* and *IL-2Rα* genes in Jurkat cells [43]. Results of these Northern hybridization experiments are shown in Figure 10A. In FR900482-treated cells, the levels of both *IL-2* (lanes 3–5) and *IL-2Rα* (lanes 3–5) mRNAs increased markedly in response

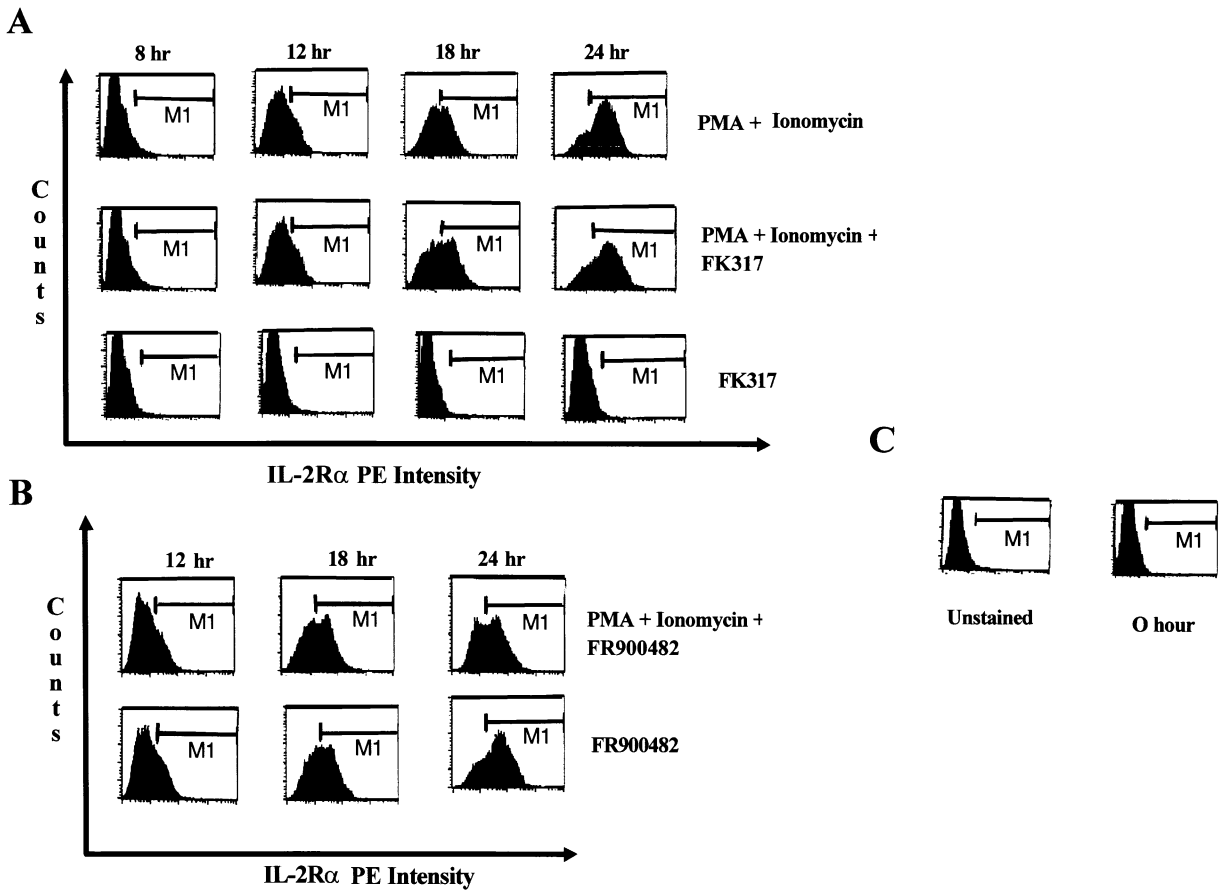

Figure 11. Flow-Cytometric Analyses of the Effects of Drug Treatment on the Time Course of Appearance of IL-2Rα Protein on the Cell Surface

(A) Jurkat cells were treated with either PMA/I alone, with FK317 (1 μM) alone, or with a combination of PMA/I plus FK317 PMA (1 μM).
(B) Jurkat cells were treated with either FR900482 (1 μM) alone or with a combination of PMA/I plus FR900482 (1 μM). At various time points (0, 8, 12, 18, and 24 hr) after the initiation of an experiment, cells were probed for the presence of surface IL-2Rα protein by reaction with an anti-IL-2Rα antibody labeled with the red-fluorescing dye phytoeryothrin (PE), and antibody binding was assessed by flow cytometry. An increase in red fluorscence (in the region marked M1) is indicative of increased IL-2Rα protein on the outer surface of the cytoplasmic membrane.
(C) Control experiments showing that both unstained Jurkat cells and Jurkat cells fixed immediately after antibody addition (0 hr samples) have an intrinsic, naturally occurring red fluorescence whose peak lies to the left of the M1 region characteristic of surface-fluorescing IL-2Rα protein. As discussed in the text, these results demonstrate two important points, namely that (1) the FR900482 drug alone (but not the FK317 drug alone) induces the appearance of IL-2Rα protein on the cell surface and (2) the FK317 drug does not inhibit the PMA/I-induced appearance of IL-2Rα protein on the cell surface.

to drug treatment and were similar to levels found in cells treated with a combination of PMA and Con A (lane 1) to induce transcription of these genes. On the other hand, the levels of *IL-2* and *IL-2Rα* mRNAs did not significantly increase in cells treated with 1 μM FK317 (lanes 6–8, in each row) and remained similar to those found in untreated control cells (lane 2). Importantly, the levels of *Gapdh*, a control housekeeping gene, remained constant regardless of the treatments (Figure 10A).

Western blot analysis was performed to investigate whether the observed FR900482-induced increase of *IL-2Rα* mRNA also reflected a parallel increase in IL-2Rα protein production. For these experiments, equal amounts of protein from either control or drug-treated cells were separated by SDS-PAGE gel electrophoresis and transferred to a nitrocellulose membrane (upper part of Figure 10B). The membrane was then reacted with antibody against the IL-2Rα protein (lower part of Figure 10B). As is evident from the Western blot, the level of IL-2Rα protein in cells treated with 1 μM FK317 (lane 2) was similar to that in untreated Jurkat cells (lane 1). On the other hand, cells treated with 1 μM FR900482 (lane 3) contained even higher levels of IL-2Rα protein than cells treated with the strong inducing combination PMA/Con A (lane 4).

Because surface expression of the IL-2Rα protein is required for the formation of a functional high-affinity IL-2 receptor in activated lymphocytes, it was of considerable importance to determine whether treatment with the FR900482 or FK317 drugs influenced either the normal cytoplasmic membrane localization and/or the time of appearance of this protein on the surface of Jurkat cells that were activated by PMA/ionomycin (PMA/I) simulation. We therefore conducted experiments (Figure 11) employing an anti-IL-2Rα antibody labeled with the red fluorescing dye phycoerythrin (PE) and flow-cytome-

tric analyses to monitor the temporal appearance of surface IL-2Rα protein on PMA/I-stimulated Jurkat cells that were treated, or not, with FK317 (1 μM) or FR900482 (1 μM) over a 24 hr period. As shown in Figure 11C, "unstained control" Jurkat cells that have never been exposed to the anti-IL-2Rα-PE antibody exhibit an intrinsic background red fluorescence due to the presence of the dye phenol red in the cell culture media, and this level of endogenous background fluorescence didn't appreciably change when "0 hr" experimental cells were briefly exposed to the anti-IL-2Rα-PE antibody. However, as shown in Figure 11A, the number of Jurkat cells expressing surface IL-2Rα protein increased as a function of time after PMA/I stimulation, as evidenced by the fact that their intensity of red fluorescence staining increased (in the region marked "M1" in the cytometric histograms) as a result of anti-IL-2Rα-PE antibody binding. These flow cytometry analyses indicate that IL-2Rα protein first appears on the surface of cells less than 8 hr after PMA/I treatment (the earliest point analyzed) and that by 12 hr post-stimulation many of the cells are expressing appreciable quantities of surface protein. Furthermore, the results also show that the time course of appearance of surface IL-2Rα protein in cells treated with a combination of both PMA/I and FK317 was approximately the same as that in cells treated with PMA/I alone. Most interestingly, it is clear from these analyses that FK317 does not aberrantly induce the surface expression of IL-2Rα in unstimulated Jurkat cells, nor does it inhibit the surface induction of this protein in cells that have been stimulated with PMA/I. In contrast, those cells treated with FR900482 alone (Figure 11B) did exhibit an aberrant induction of the expression of surface IL-2Rα protein, but the drug had no noticeable effect on the induction of surface protein expression in cells treated with PMA/I.

The results from these various lines of investigation therefore allow us to conclude that the FR900482 drug, in contrast to FK317, upregulates the levels of expression of *IL-2Rα* mRNA in Jurkat cells which, in turn, leads to increased cellular concentrations and surface expression of the IL-2Rα protein. In this connection, it is interesting to note that Li et al. [44] have recently reported that necrotic cell death results in the upregulation of NF-κB, a transcription factor that is involved in the regulation of both *IL-2* and *IL-2Rα* genes, a finding that is consistent with our present results. It is tempting to speculate that the minor structural differences between FR900482 and FK317, especially the presence of the methyl group on FK317, are responsible for the observed differences in their biological effects. The detailed chemical mechanistic underpinning of this phenomenon is not presently understood and is the subject of ongoing investigation.

Significance

The FR900842 and FK317 drugs share several biochemical and pharmacological properties, including the ability to induce DNA-DNA interstrand crosslinks, minor-groove DNA-protein crosslinks, and similar (but slightly different) cellular toxicities. These properties are likely to be a common feature of most FR900482 derivatives. Nevertheless, here we report that the two drugs exhibit several important biological differences. The first is a difference in the mode of cell death induced by the two drugs. The type of cell death induced by chemotherapeutic agents is important because a necrotic cell death can lead to serious side effects such as VLS, whereas apoptotic cell death is less detrimental. Earlier, we reported that FR900482 induces necrotic cell death [13]. In contrast, we now report that FK317 induces necrosis at low drug concentrations and apoptosis at high concentrations. One possible explanation for this therapeutically beneficial necrosis-apoptosis switch is that a change in the Bcl-2 homodimer/heterodimer ratio occurs at higher FK317 drug concentrations. The second important biological difference between these two drugs is that FR900482, but not FK317, induces both *IL-2* and *IL-2Rα* gene expression. The upregulation of *IL-2* and *IL-2Rα* by FR900482 could easily explain why FR900482 induces VLS and FK317 does not. After metabolic processing inside the cell, the active metabolites of FK317 and FR900482 differ by only one methyl group on the C5 phenolic oxygen atom. Given their noticeably different biological effects, it will be informative to determine whether the additional methyl group of FK317 mandates significant structural differences in the way the drugs crosslink proteins to the minor groove of DNA.

Experimental Procedures

Cell Culture

Human Jurkat T-leukemia cells (clone E6-1; American Type Culture Collection, Rockville, MD) were grown in RPMI-1640 media (Gibco-BRL, Rockville, MD) supplemented with 5% Fetal Bovine Serum (Atlanta Biologicals, Norcross GA), penicillin (614 ug/ml, Sigma, St. Louis, MO), streptomycin (10 ug/ml, Sigma St. Louis, MO), and HEPES buffer (pH 7.2) at 37°C and 5% CO_2. Jurkat cells overexpressing Bcl-2 [40] were a generous gift from Dr. S.J. Korsmeyer and were maintained as for the Jurkat cells.

Growth Inhibition and Viability Assays

Jurkat cells were plated at 5×10^6 cells per plate and grown for 24 hr. Subsequently, FK317 was added at 0, 0.5, 1, and 1.5 μM concentrations. Cells were counted every 24 hr for the next 72 hr on a hemocytometer. Trypan Blue (2%) was added to the cells to determine cell viability. To determine the total number of live cells, the number of blue cells (dead cells) was subtracted from the total number of cells. This number was then plotted as a function of time with Excel.

Chromatin Immunopreciptation Assays (ChIP)

ChIP assays were done as previously reported [12]. In brief, 1×10^7 Jurkat cells were left untreated, treated for 24 hr with 0.5 μM FK317 at 37° and 5% CO_2, or treated for 30 min with 1% formaldehyde at room temperature. Cells were then harvested by centrifugation. Nuclei were isolated with a buffer containing 0.34 M sucrose, 0.2 M KCl, 100 mM EGTA, 500 mM EDTA, 494 mM spermine, 689 mM spermidine, 10 mM HEPES, and 5% NP-40. The nuclei were washed in the same buffer without NP-40. The nuclei were then fragmented by sonication to produce chromatin fragments containing, on average, about 400–500 bp of DNA. The DNA was extracted by the use of phenol:chloroform:isoamyl alcohol (25:24:1) and was ethanol precipitated. The DNA was then subsequently redissolved in 1× PBS, and HMGA1, Elf-1 (Santa Cruz Biotechnology, Santa Cruz, CA), or NF-κB p50 (Santa Cruz Biotechnology, Santa Cruz CA) antibodies were added at a 50:1 ratio. The reaction was allowed to proceed overnight at 4°C, after which Protein A Sepharose beads (10:1) were

added. The DNA-protein crosslinks were then isolated by centrifugation and collection of Protein A Sepharose beads. The beads were then redissolved in 1× PBS and 5 μg Proteinase K and incubated overnight at 55°C. The DNA from the samples was extracted by the use of phenol:choloroform:isoamyl alcohol (25:24:1). DNA was then ethanol precipitated and redissolved in water. PCR primer sequences for the IL gene promoter (accession number J006884) are as follows: IL-2-1 (sense), 5′-TAATGTAACAAGAGGGATTTC ACC-3′ (base pairs 193–217); and IL-2-2 (antisense), 5′-GGAGTTGA GGTTACTGTGAGTAGTC-3′ (base pairs 450–427). PCR primer sequences for the IL-2Rα gene promoter (accession number M15864) are as follows: IL-2R-1 (sense), 5′-CCAGCCCACACCTCCAG CAA-3′ (base pairs 1052–1071); and IL-2R-2 (antisense), 5′-CCTCT TTTTGGCATCGCGCCG-3′ (base pairs 1306–1327). PCR conditions were 0.5 mM dNTPs, 2 μM primers, 4 mM $MgCl_2$, 100 mM Tris (pH 9.0), 50 mM KCl, 1% Triton X-100, and 1 mM DTT. Taq polymerase was used with 35 cycles of 96°C for 30 s, 58°C (*IL-2R* primers) or 52°C (*IL-2* primers) for 30 s, and 72°C for 45 s. The PCR samples were run on a 1% agarose gel.

Mode of Cell Death Determination

Jurkat cells (1×10^7) were treated with either 1, 10, or 100 μM FK317 or 1, 10, or 100 μM FR900482 (Fujisawa Pharmaceuticals) for 24, 48, or 72 hr. Cells were then split into two separate groups and pelleted by centrifugation. One group of cells was resuspended in 1× PBS and placed on poly-L-lysine (Sigma, St. Louis, MO)-coated slides and fixed in formol alcohol (70% ethanol, 1.5% formaldehyde, 1.5% acetic acid). Cells were stained in Gill's Hemotoxylin and counterstained in Geimsa. The cells were then viewed with a compound microscope at 100× magnification. The other group of cells was used for flow cytometry analysis. Cells were treated with Annexin-V-FITC (1:50 ratio, Caltag Laboratories, Burlingame, CA) in Annexin-V binding buffer (10 mM HEPES, 140 mM NaCl, 5 mM KCl, 1 mM $MgCl_2$, and 2.5 mM $CaCl_2$) and incubated on ice for 10 min. The binding reaction was stopped by the addition of excess binding buffer. Propidium iodide (1:10 ratio of 1 mg /ml solution, Calbiochem, La Jolla, CA) was added to the reaction, and flow cytometry analysis was performed with CellQuest (BD Biosciences, San Jose, CA).

TUNEL Analysis

TUNEL assays were performed with the Apoptosis Detection System, Fluorescein kit (Promega, Madison, WI). In brief, Jurkat cells (3×10^7) were spread on a poly-L-lysine slide (Sigma, St. Louis, MO), washed in phosphate-buffered saline (PBS), fixed with 4% paraformaldehyde, and permeabilized with 0.2% Triton X-100. The cells were incubated with 50 μM flourescein-12-dUTP, equilibration buffer (supplied with the kit), and terminal deoxynucleotidyl transferase (TdT) for 1 hr at 37°C. The reaction was stopped by washing the cells in 2× SSC followed by washing twice in PBS. The cells were counterstained with 1 mg/ml propidium iodine and washed in dH_2O. The cells were analyzed with a fluorescence microscope. Cells that displayed green fluorescence were indicative of DNA fragmentation due to labeling by fluorescein-12-dUTP by TdT.

Caspase 3 and 7 Activation Assays

Jurkat cells (1×10^6) were either left untreated or treated with 1 or 10 μM of either FK317 or FR900482 for 24 hr. Cells were harvested and incubated with 5 μl fetal bovine serum (Atlanta Biologicals, Norcross, GA) and 50 μl Phi Phi Lux (OncoImmunin, Inc, Gaithersburg, MD) for 1 hr at 37°C. After incubation was complete, the reaction was stopped by the addition of 1 ml flow cytometry buffer, and cells were harvested. The cells were then resuspended in 1 ml flow cytometery buffer and 4 μl propidium iodide (1:10 ratio of 1 mg/ml solution, Calbiochem, La Jolla, CA). Flow-cytometric analysis was done with CellQuest (BD Biosciences, San Jose, CA) immediately after PI addition.

Northern Blot Analysis

RNA was isolated from Jurkat cells (1×10^7) treated with 1, 10, or 100 μM FK317 or either 1 or 100 μM FR900482 for 6, 12, or 24 hr by the use of Triazol reagent (Gibco-BRL, Rockville, MD). For a positive control of induction of *IL-2* and *IL-2Rα*, RNA from cells treated with PMA (10 nM) and Con A (10 μM) for 24 hr was isolated. RNA was run out on a 6% formaldehyde, 1% agarose-MOPS gel for 4.5 hr at 100 V. The RNA was transferred onto Supercharge Nylon Membrane (Schleicher and Schuell, Keene, NH) in 20× SSC. The blot was dried, rinsed in 5× SSC, and prehybridized in PerfectHybPlus (Sigma, St. Louis, MO) and salmon sperm DNA (25 μg/ml) for 1 hr at 65°C. The processed membranes were hybridized with one or more of the following oligonucleotide probes derived from human gene sequences: *GAPDH* (1200 bp cDNA, Genbank accession number M33197); *IL-2* (190 bp fragment from the gene 3′ UTR, Genbank accession number M00586); *IL-2Rα* (220 bp fragment from Exon 1, Genbank accession number M15864); and *Bcl-2* (450 bp cDNA, Genbank accession number M000633). The hybridization probes were ^{32}P-radiolabeled by random priming procedures as previously described [16], and in each reaction, approximately 10 ng/ml of 10^8 dpm/μg probe was added to the prehybrization mix incubated overnight at a hybridization temperature appropriate for the probe. The hybridized blots were washed in 2× SSC and 0.1% SDS for 10 min at room temperature, and phosphoimager anaylsis was done (Molecular Dynamics, Sunnyvale, CA).

Western Blot Analysis

Jurkat cells were either treated with 1 μM FK317, 1 μM FR900482, or both PMA (10 nM) and Con A (10 μM) or left untreated for 24 hr. Cells were then harvested by centrifugation, resuspended in SDS-PAGE buffer (10% glycerol, 5% 2-mercaptoethanol, 10% SDS, 0.625 M Tris, and 0.1% bromophenol blue), and sonicated for 3 min. Samples were heated to 95°C and placed immediately on ice. Proteins were then separated by SDS-PAGE by the use of duplicate 18% SDS-PAGE gels with a 3% SDS-PAGE stacking gel. Protein Molecular Weight Marker (Fermentas, Hanover MD) was used for determination of molecular weights. One gel was transferred onto Immobilin-P membrane (Millipore, Bedford, MA) via the semidry transfer method by the use of transfer buffer (48 mM Tris, 39 mM glycine, 0.037% SDS, and 20% methanol). The transfer was allowed to proceed for 2 hr at 0.8 mA per cm^2 of membrane. After transfer, the membrane was wetted in methanol, rinsed in water, and blocked in PBS-T plus 1% dried milk. The membrane was then incubated for 1 hr, and IL-2Rα antibody (Santa Cruz Biotechnology, Santa Cruz, CA; 100:1) was added. The incubation then continued overnight. The membrane was rinsed extensively in 1× PBS-T. The membrane was then incubated in PBS-T plus 1% dried milk and goat antimouse IgG HRP conjugate secondary antibody (BioRad Laboratories, Richmond, CA) for 1 hr. The membrane was again rinsed extensively in 1× PBS-T, after which chemiluminescence (Pierce, Rockford, IL) was performed to detect labeling. The second gel was stained in Coomassie blue stain (0.04% Coomassie brilliant blue, 10% acetic acid, and 25% isopropanol) for 1 hr and destained (10% methanol, 10% acetic acid, and 1% glycerol) overnight.

Flow Cytometric Analysis of IL-2Rα on the Cell Surface

Jurkat cells (1×10^6) were treated with PMA (10 nM) and ionomycin (10 μM) for 0, 1, 2, 4, 8, 12, 18, or 24 hr; treated with PMA (10 nM), ionomycin (10 μM), and 1 μM FK317 for 0, 1, 2, 4, 8, 12, 18 or 24 hr; treated with 1 μM FK317 for 0, 1, 2, 4, 8, 12, 18, or 24 hr; or left untreated. Cells were pelleted after incubation, washed with 1× PBS, and incubated in 1× PBS and anti CD25-PE-labeled antibody (1:3, BD Pharmingen, San Jose, CA) on ice for 30 min. Cells were pelleted, washed with 1× PBS, and fixed in 2% paraformaldehyde. Flow-cytometric analysis was done with CellQuest (BD, Biosciences, San Jose, CA).

Acknowledgments

We thank Fujisawa Pharmaceutical Company, Japan for the generous gift of FR900482 and FK317 and Dr. S.J. Korsmeyer for the gift of the GADPH and Bcl-2 cDNAs and Jurkat cells overexpressing Bcl-2. Financial support by National Institutes of Health grants CA51875 (R.M.W.) and GM46352 (R.R.) is gratefully acknowledged.

Received: June 28, 2001
Revised: January 7, 2002
Accepted: January 17, 2002

References

1. Baluna, R., Rizo, J., Gordon, B.E., Ghetie, V., and Vitetta, E. (1999). Evidence for a structural motif in toxins and interleukin-2 that may be responsible for binding to endothelial cells and initiating vascular leak syndrome. Proc. Natl. Acad. Sci. USA *96*, 3957–3962.
2. Rafi-Janajreh, A.Q., Chen, D., Schmits, R., Mak, T.W., Grayson, R.L., Sponenberg, D.P., Nagarkatti, M., and Nagarkatti, P.S. (1999). Evidence for the involvement of CD44 in endothelial cell injury and induction of vascular leak syndrome by IL-2. J. Immunol. *163*, 1619–1627.
3. Baluna, R., and Vitetta, E. (2001). Vascular leak syndrome: a side effect of immunotherapy. Immunopharmacology *37*, 117–132.
4. Teelucksingh, S., Padfield, P.L., and Edwards, C.R.W. (1990). Systemic capillary leak syndrome. Q. J. Med. *75*, 515–524.
5. Barnadas, M.A., Cisteros, A., Dolors, S., Pascual, E., Puig, X., and de Moragas, J.M. (1995). Systemic capillary leak syndrome. J. Am. Acad. Dermatol. *32*, 364–366.
6. Naoe, Y., Inami, M., Matsumotot, S., Takagaki, S., Tomoichi, F., Yamazaki, T., Kawamura, I., Nishigaki, F., Tsujimoto, S., Manda, T., et al. (1998). FK317, a novel substituted dihydrobenzoxazine, exhibits potent antitumor activity against human tumor xenografts in nude mice. Jpn. J. Cancer Res. *89*, 1306–1317.
7. Naoe, Y., Inami, M., Kawamura, I., Nishigaki, F., Tsujimoto, S., Matsumoto, S., Manda, T., and Shimomura, K. (1998). Cytotoxic mechanisms of FK317, a new class of bioreductive agents with potent antitumor activity. Jpn. J. Cancer Res. *89*, 666–672.
8. Naoe, Y., Inami, M., Takagaki, S., Matsumotot, S., Kawamura, I., Nishigaki, F., Tsujimotot, S., Manda, T., and Shimomura, K. (1998). Different effects of FK317 on multidrug-resistant tumors *in vivo* and *in vitro*. Jpn. J. Cancer Res. *89*, 1047–1054.
9. Denny, W.A. (1995). Hypoxia-selective cytototoxins. In Cancer Chemotheurpeutic Agents, W.O. Foye, ed. (Washington, DC: ACS Press), pp. 483–500.
10. Paz, M.M., and Hopkins, P.B. (1997). DNA-DNA interstrand crosslinking by FR66979 and FR900482: requirement of metal ions during reductive activation. Tetrahedron Lett. *38*, 343–346.
11. Paz, M.M., and Hopkins, P.B. (1997). DNA-DNA interstrand crosslinking by FR66979: intermediates in the activation cascade. J. Am. Chem. Soc. *119*, 5999–6005.
12. Fukuyama, T., and Goto, S. (1989). Synthetic approaches toward FR900482. I. Stereoselective synthesis of a pentacyclic model compound. Tetrahedron Lett. *30*, 6491–6494.
13. Beckerbauer, L., Tepe, J.J., Cullison, J., Reeves, R., and Williams, R.M. (2000). New FR900482 class of anti-tumor drugs cross-links oncoprotein HMG I/Y to DNA in vivo. Chem. Biol. *7*, 805–812.
14. Fredholt, K., Adrian, C., Just, L., Larsen, D.H., Weng, S., Moss, B., and Friis, G.J. (2000). Chemical and enzymatic stability as well as transport properties of a Leu-enkephalin analogue and ester prodrugs thereof. J. Controlled Release *63*, 261–273.
15. Bustin, M. (2001). Revised nomenclature for high mobility group (HMG) chromosomal proteins. Trends Biochem. Sci. *26*, 152–153.
16. John, S., Reeves, R., Lin, J.X., Child, R., Leiden, J.M., Thompson, C.B., and Leoni, L. (1995). Regulation of cell-type-specific interleukin-2 receptor alpha-chain gene expression: potential role of physical interactions between Elf-1, HMG-I(Y), and NF-kappa B family proteins. Mol. Cell. Biol. *15*, 1786–1796.
17. John, S., Robbins, C.M., and Leonard, W.J. (1996). An IL-response element in the human IL-2 receptor alpha chain promoter is a composite element that binds Stat5, Elf-1, HMG-I(Y) and a GATA family protein. EMBO J. *15*, 5627–5635.
18. Himes, S.R., Coles, L.S., Reeves, R., and Shannon, M.F. (1996). High mobility group protein I(Y) is required for function and for c-Rel binding to CD28 response elements within the GM-CSF and IL-2 promoters. Immunity *5*, 479–489.
19. Williams, R.M., Rajski, S.R., and Rollins, S.B. (1997). FR900482, a close cousin of mitomycin C that exploits mitosene-based DNA cross-linking. Chem. Biol. *4*, 127–137.
20. Strasser, A., O'Conner, L., and Dixit, V.M. (2000). Apoptosis signaling. Annu. Rev. Biochem. *69*, 217–245.
21. Earnshaw, W., Martins, L.M., and Kaufman, S.H. (1999). Mammalian caspases: structure, activation, substrates, and functions during apoptosis. Annu. Rev. Biochem. *68*, 383–424.
22. Kroemer, G., Dallaporta, B., and Resche-Rigon, M. (1998). The mitochondrial death/life regulator in apoptosis and necrosis. Annu. Rev. Physiol. *60*, 619–642.
23. Savill, J., and Bebb, C. (2000). Apoptotic cell phagocytosis. Handbook of Experimental Pharmacology *142*, 151–177.
24. Cameron, R., and Feuer, G. (2000). Incidence of apoptosis and its pathological and biochemical manifestations. Handbook of Experimental Pharmacology *142*, 3–35.
25. Koopman, G., Reutelingsperger, C.P.M., Kuijten, G.A.M., Keehnene, R.M.J., Pals, S.T., and van Oers, M.H.J. (1994). Annexin V for flow cytometric detection of phosphatidylserine expression on B cells undergoing apoptosis. Blood *84*, 1415–1420.
26. Vermes, I., Haanen, C., and Reutelingsperger, C.P.M. (2000). Flow cytometry of apoptotic cell death. J. Immunol. Methods *243*, 167–190.
27. Palomba, L., Sestili, P., Columbaro, M., Falcieri, E., and Cantoni, O. (1999). Apoptosis and necrosis following exposure of U937 cells to increasing concentrations of hydrogen peroxide: the effect of the poly (ADP-ribose)polymerase inhibitor 3-aminobenzamide. Biochem. Pharmacol. *58*, 1743–1750.
28. McConkey, D.J. (1998). Biochemical determinants of apoptosis and necrosis. Toxicol. Lett. *99*, 157–168.
29. Eguchi, Y., Shimizu, S., and Tsujimoto, Y. (1997). Intracellular ATP levels determine cell death fate by apoptosis and necrosis. Cancer Res. *57*, 1835–1840.
30. Hirsch, T., Marchetti, P., Susin, S.A., Dallaporta, B., Zamzxami, N., Marzo, I., Geuskens, M., and Kroemer, G. (1997). The apoptotsis-necrosis paradox. Apoptogenic proteases activated after mitochondrial permeability transition determine the mode of cell death. Oncogene *15*, 1573–1581.
31. Desagher, S., Osen-Sand, A., Montessuit, S., Magnenat, E., Vilbois, F., Hochmann, A., Journot, L., Antonsson, B., and Marinou, J. (2001). Phosphorylation of Bid by casein kinase I and II regulates its cleavage by caspase 8. Mol. Cell *8*, 601–611.
32. McDonnell, T.J., Beham, A., Sarkiss, M., Anersen, M., and Lo, P. (1996). Importance of the Bcl-2 family in cell death regulation. Expermentia *52*, 1008–1017.
33. Park, J.W., Choi, Y., Suh, S., Baek, W., Suh, M., Jin, I., Min, D., Woo, J., Chang, J., Passaniti, A., et al. (2001). Bcl-2 overexpression attenuates resveratrol-induced apoptosis in U937 by inhibition of caspase-3 activity. Carcinogenesis *25*, 1633–1639.
34. Oltvai, Z., Milliman, C.L., and Korsmeyer, S.J. (1993). Bcl-2 heterodimerizes in vivo with a conserved homology Bax, that accelerates programmed cell death. Cell *74*, 609–619.
35. Guchelaar, J.J., Vermes, A., Vermes, I., and Haanen, C. (1997). Apoptosis: molecular mechanisms and implications for cancer chemotherapy. Pharm. World Sci. *19*, 119–125.
36. Allen, R.T., Cluck, M.W., and Agrawal, D.K. (1998). Mechanisms controlling cellular suicide: role of Bcl-2 and caspases. Cell. Mol. Life Sci. *54*, 427–445.
37. Crawford, M.J., Krishnamoorthy, R.R., Rudick, V.L., Collier, R.J., Kapin, M., Aggarwal, B.B., Al-Ubaidi, M.R., and Agarwall, N. (2001). Bcl-2 overexpression protects photooxidative stress-induced apoptosis of photorecpetor cells via NF-κB preservation. Biochem. Biophys. Res. Commun. *281*, 1304–1312.
38. Shilkaitis, A., Graves, J., Mehta, R.R., Hu, L., You, M., Lubet, R., Steele, V., Kelloff, G., and Christov, K. (2000). Bcl-2 and Bax are differentially expressed in hyperplastic, premalignant, and malignant lesions of mammary carcinogenesis. Cell Growth Differ. *11*, 437–445.
39. Johnson, B.L., Cooper, I.R., Jenkins, J.R., and Chow, S.C. (1999). Effects of differential overexpression of Bcl-2 on apoptosis, proliferation, and telomerase activity in Jurkat T cells. Exp. Cell Res. *251*, 175–184.
40. Yamamoto, K., Ichijo, H., and Korsmeyer, S.J. (1999). Bcl-2 is phopshorylated and inactivated by an ASK1/Jun N-terminal protein kinase pathway normally activated at G2/M. Mol. Cell. Biol. *19*, 8469–8478.
41. Kaplan, G., Cohn, Z.A., and Smith, K.A. (1992). Rational immunotherapy with interleukin 2. Biotechnology *10*, 157–162.

42. Lentsch, A.B., Miller, F.N., and Edwards, M.J. (1999). Mechanisms of leukocyte-mediated tissue injury induced by interleukin 2. Cancer Immunol. Immunother. *47*, 243–248.
43. Gillis, S., and Watson, J. (1980). Biochemical and biological characterization of lymphocyte regulatory molecules. J. Exp. Med. *152*, 1709–1719.
44. Li, M., Carpi, D.F., Zheng, Y., Bruzzo, P., Singh, V., Ouaaz, F., Medzhitov, R.M., and Beg, A.A. (2001). An essential role of the NF-κB/Toll-like receptor pathway in induction of inflammatory and tissue-repair gene expression by necrotic cells. J. Immunol. *166*, 7128–7135.